

Grasping Without Squeezing: Design and Modeling of Shear-Activated Grippers

Elliot Wright Hawkes¹, *Member, IEEE*, Hao Jiang², *Student Member, IEEE*,
David L. Christensen, *Student Member, IEEE*, Amy K. Han³, *Student Member, IEEE*,
and Mark R. Cutkosky⁴, *Fellow, IEEE*

Abstract—Grasping objects that are too large to envelop is traditionally achieved using friction that is activated by squeezing. We present a family of shear-activated grippers that can grasp such objects without the need to squeeze. When a shear force is applied to the gecko-inspired material in our grippers, adhesion is turned on; this adhesion in turn results in adhesion-controlled friction, a friction force that depends on adhesion rather than a squeezing normal force. Removal of the shear force eliminates adhesion, allowing easy release of an object. A compliant shear-activated gripper without active sensing and control can use the same light touch to lift objects that are soft, brittle, fragile, light, or very heavy. We present three grippers, the first two designed for curved objects, and the third for nearly any shape. Simple models describe the grasping process, and empirical results verify the models. The grippers are demonstrated on objects with a variety of shapes, materials, sizes, and weights.

Index Terms—Bioinspiration, dry adhesives, grasping.

Manuscript received May 2, 2017; revised August 11, 2017; accepted November 2, 2017. Date of publication December 25, 2017; date of current version April 12, 2018. This paper was recommended for publication by Associate Editor S. Bergbreiter and Editor I.-M. Chen upon evaluation of the reviewers' comments. This work was supported in part by NASA under Grant ESI NNX16AD19G, in part by Army Research Laboratory's Micro Autonomous System and Technologies under Project MCE 15-4.4, and in part by Ford Motor Company: "Bio-Inspired Adhesion for Manufacturing Aids." This paper was presented in part at the 2015 IEEE International Conference on Robotics and Automation, Washington State Convention Center, Seattle, WA, USA, May 2015 [14]. (*Corresponding author: Elliot Wright Hawkes.*)

E. W. Hawkes is with the Department of Mechanical Engineering, University of California, Santa Barbara, Santa Barbara, CA 93106 USA (e-mail: ewhawkes@engineering.ucsb.edu).

H. Jiang, D. L. Christensen, A. K. Han, and M. R. Cutkosky are with the Department of Mechanical Engineering, Stanford University, Stanford, CA 94305 USA (e-mail: jianghao@stanford.edu; dleboy@gmail.com; kwhan@stanford.edu; cutkosky@stanford.edu).

This paper has supplementary downloadable material available at <http://ieeexplore.ieee.org>, provided by the author. The material consists of a video (.mp4 format) that shows the shear-activated grippers lifting a variety of objects, along with explanatory content about how they work. This video first introduces the concept of shear-activated grippers. Gecko-inspired adhesives turn on when loaded in shear, but turn off when not loaded. The authors then present three devices. The first device is the Simple Curved Surface Gripper, which uses a bistable frame that collapses to allow the film to conform and grasp objects. The second device is the Gripper with Moment Ability. It has a C-shaped frame between the two films, allowing the gripper to apply moments to the object. Finally, they show the Lateral Gripper, which has two air-filled bladders that help conform the adhesive film to the object. The size of the video is 57 MB. Contact ewhawkes@engineering.ucsb.edu for further questions about this work.

Color versions of one or more of the figures in this paper are available online at <http://ieeexplore.ieee.org>.

Digital Object Identifier 10.1109/TRO.2017.2776312

I. INTRODUCTION

TRADITIONAL grasping uses normal forces to hold objects. If an object is small relative to the gripper, the gripper envelops the object and applies normal forces to support it (form closure); for larger objects, the gripper squeezes the object and creates load-controlled friction to hold it (force closure) [1]. Often, both direct support and friction hold the object. While load-controlled friction is very useful for grasping objects, it has two drawbacks: The squeezing normal force can crush delicate or deformable objects, and the normal force tends to push objects out of the grasp in the case where the gripper cannot reach at least halfway around the object. Examples of such grippers are numerous, including rigid and fully actuated ones [2]–[4], as well as more compliant, underactuated, and back drivable grippers [5]–[7]. Extensive reviews are provided in [8] and [9].

There exist a number of alternatives to traditional grippers. Vacuum is often used in manufacturing for lifting nonporous objects without readily graspable features. Vacuum can be combined with particle jamming and friction to grasp a variety of objects [10]. A mushroom-tipped adhesive that is sticky in its default state can use normal adhesion to lift objects once it is pressed onto the surface, and is able to lift 0.4 N at ≈ 2 kPa [11]. These examples use primarily a normal force that is directed away from the object to lift it. Electrostatic adhesion requires much less pressing force to engage but provides limited adhesion that would require a very large piece and additional control infrastructures for large load applications [12], [13].

Here, we present a family of shear-activated grippers¹ that work differently from traditional grippers and the above-mentioned alternative grippers. These devices grip an object when a shear load is applied to the gecko-inspired adhesive material on the surface of the gripper. A shear-activated gripper is able to grasp large, deformable, or delicate objects without squeezing (see Fig. 1).

In this paper, we first describe the concept behind shear-activated grippers, and then we describe three gripper versions. We develop models of the adhesive film and each of the three grippers. In Section V, we verify each of the models, show how the adhesive material is able to self-engage on textured glass

¹A single example case has been extended to a general concept of shear-activated grippers. Further, two new devices are introduced, along with models and experiments, allowing the application of moments as well as grasping of a much greater range of objects.



Fig. 1. Flexible shear-activated gripper holds a water-filled bag. Load tendon is at center; outer tendons release the adhesive film.

when loaded in shear, and demonstrate implementations of two of the designs for grasping tasks, including catching ballistic objects. Finally, we discuss implications of the work, conclude, and suggest future directions.

II. CONCEPT OF SHEAR-ACTIVATED GRIPPERS

A. Traditional Grippers

When examining human grasping, or traditional robotic grasping which emulates it, load-controlled friction is a dominant force when the object is too large for the gripper to envelop it. Load-controlled friction is the familiar friction force between two surfaces that depends on the normal load applied to the interface between the surfaces [15]. Squeezing the sides of an object creates the load-controlled friction that acts tangent to the surface to lift the object. This friction is remarkably useful when considered; it acts nearly instantly, is not easily fouled by dirt or dust, and is turned on or off as the normal load is applied or removed.

Load-controlled friction also has drawbacks. Because it is controlled by an applied normal force, squeezing is required. This squeezing can deform a soft object, such as a ripe tomato, or break a fragile object. Further, for relatively large objects that a gripper cannot reach at least half of the way around, e.g., a basketball that a human is attempting to grasp, the normal forces are actually pushing the object out of the grasp.

B. Shear-Activated Grippers

We propose the concept of shear-activated grippers, which avoid these drawbacks found in traditional grippers using load-controlled friction. Shear-activated grippers are based on a fibrillar, gecko-inspired material that has adhesion that is turned “on”

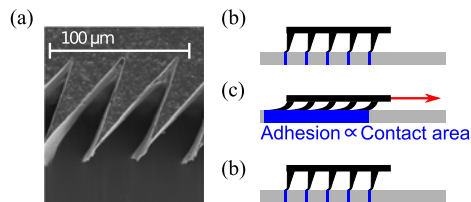


Fig. 2. (a) Micrograph of the microwedge adhesive material. Details of manufacturing are found in [18] and [19]. (b) Tips of the microwedge adhesive self-engage with a surface when brought in contact. (c) When loaded in shear, the wedges lay over, and a large real area of contact produces adhesion. (d) When the shear load is relaxed, the stored elastic energy in the wedges lifts them from the surface, allowing them to be removed easily.

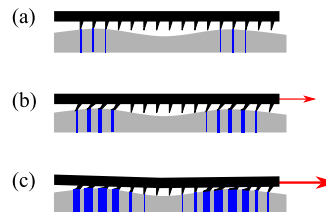


Fig. 3. (a) On a wavy surface, the tips of the microwedge adhesive self-engage only at the highest points. (b) When loaded in shear, the wedges lay over, pulling more wedges into contact. (c) More shear increases this effect.

by the applied shear load, and “off” by the removal of the shear load (see Fig. 2) [16]. Turning on the adhesion in turn results in adhesion-controlled friction. Adhesion-controlled friction is a less familiar form of friction that depends on the adhesion between two surfaces [15]. The adhesion and thus the adhesion-controlled friction can be turned on quickly, reaching 80% of maximum capacity in only 68 ms [17]. In summary, a shear load activates adhesion, and adhesion activates adhesion-controlled friction; with this friction, we can grasp objects without squeezing.

The mechanics of the microwedge adhesive employed allow the application of shear load to increase the adhesion and thus the adhesion-controlled friction force even on a wavy surface (see Fig. 3). A few wedges will self-engage with the high points of the surface when brought in contact. As the shear load is increased, these wedges will lay over, bringing their neighbors closer to the surface. More wedges will engage, and the effect propagates. Experiments showing this effect are presented in Section V-B3.

III. DESIGNS

In previous work, we introduced a simple shear-activated gripper for curved surfaces [14]. We briefly describe this design, then we introduce a new design that builds on the curved surface gripper to allow the application of moments to the gripped object. We then present a third design, the lateral gripper, which is capable of lifting a much larger variety of objects than either of the previous designs.

A. Simple Curved Surface Gripper

The design of the curved surface gripper is shown in Fig. 4. A thin flexible adhesive is held taut between two ends of a bistable

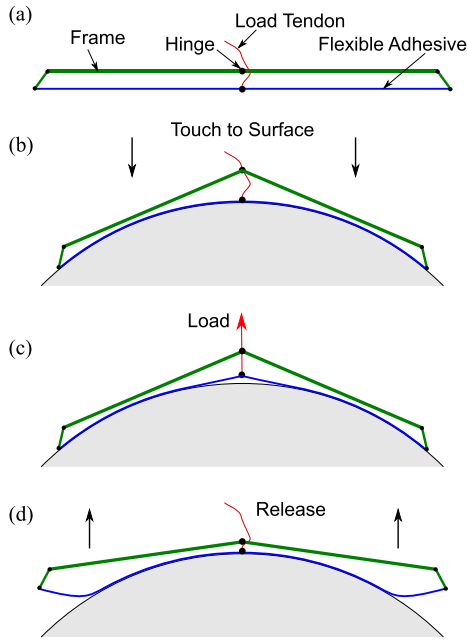


Fig. 4. (a) Key components of the curved surface gripper are shown, including a bistable frame that holds the flexible adhesive film taut. (b) Frame collapses when the device touches a curved surface, allowing the film to conform. (c) When tension is applied to the load tendon, the adhesives are turned on, and the object is gripped. (d) Removing tension turns the adhesive off, and the device can detach easily from the surface.

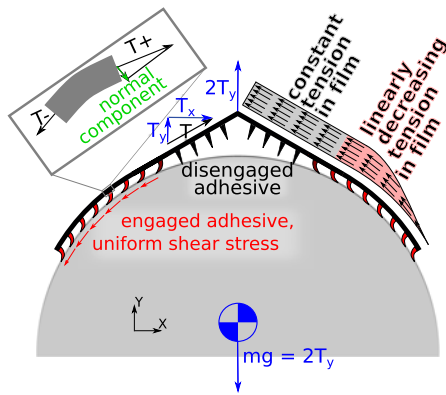


Fig. 5. Forces present during grasping with the curved surface gripper.

frame. As the frame is touched to a curved surface it collapses, and the adhesive makes contact with the surface. When a force is applied to the load tendon, the adhesive is sheared and adhesion, along with adhesion-controlled friction, results. When the force is removed from the load tendon, the adhesion turns off. Lifting the arms of the device easily removes it.

1) *Forces in the Film*: Fig. 5 shows the forces in the film during lifting. The resultant of the forces applied to the load tendon by the film must equal the weight of the object, or $mg = 2T_y$, where T_y is the vertical component of the tension in the free section of the film, not in contact with the object. In this section of film, the tension is uniform. The horizontal component T_x is balanced by the corresponding horizontal component in the opposite side.

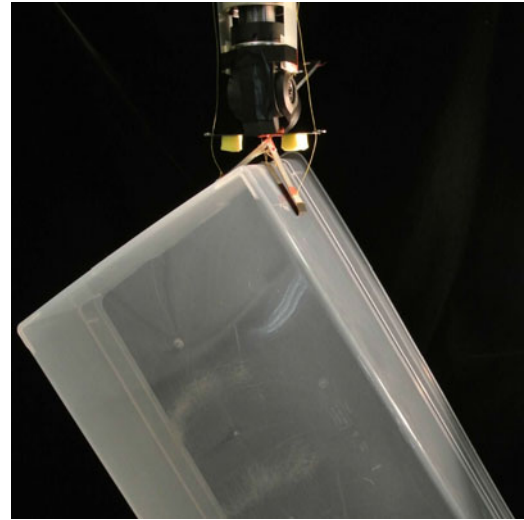


Fig. 6. Gripper can also grasp convex objects with straight sides.

Between the section of film that is in contact with the object and the surface of the object, there is an approximately uniform shear stress, assuming the adhesive is loaded near its limit, with proximal sections slipping slightly to equalize the shear stress (see Section IV-A for further explanation and Section V-A1 for data supporting this assumption). With a uniform shear stress, the tension in the film is not uniform, but decreasing distally. This decrease in tension results because tension in the film at a given point is an integration of the shear force in the film distal to the point. For example, a cross section of the film near the distal end has only the tension necessary to balance the shear force in the small section of more distal film. In contrast, a cross section of film closer to the load tendon must balance the shear force accumulated over a greater length.

Finally, there are forces in the radial direction. First, there is the adhesive force between the microwedges and the surface, which is not shown in Fig. 5 because this force is not directly used in grasping. The flexible, thin film cannot transmit a bending moment that would be necessary to exploit this normal force. However, the adhesive force is used indirectly to turn on the adhesion-controlled friction. There also exists a very small, yet still present, force due to the curvature of the loaded film. If a small section of the curved film is examined, the tension applied to either end is not in opposite directions (see Fig. 5, inset), but directed parallel to the local tangent. Therefore, there is a small normal component to the tension. This small force has the effect of bringing any area of film that is not initially in contact with the surface into full contact. The magnitude of the normal force due to the curvature of the film is quite small. For example, on an object with a 30-cm radius of curvature, its magnitude is approximately 3% of the magnitude of the shear force. Further, it is not required for grasping. As shown in Fig. 6, the gripper is capable of lifting objects with straight sides. In this case, there is no curvature, and the discussed force is not present.

2) *Bistable Frame*: It is desirable to hold the film taut before contact to prevent wrinkles from forming after contact. It is

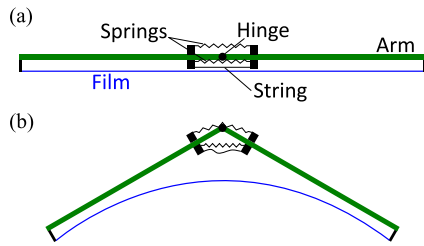


Fig. 7. (a) Details of the bistable frame. (b) Beyond a critical angle, the frame snaps into the collapsed state.

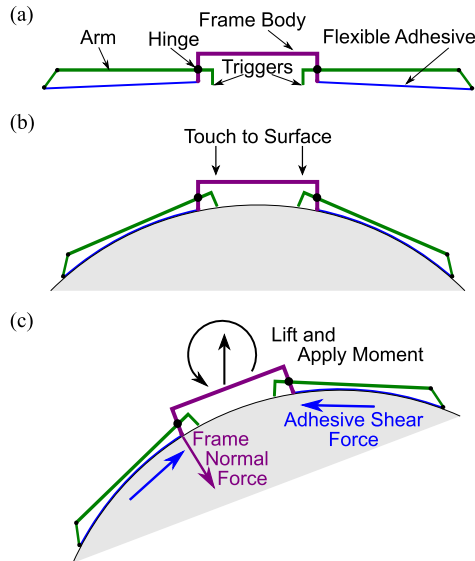


Fig. 8. (a) Design of a gripper with moment ability. An independent frame body is added between the two arms, to which the proximal ends of the flexible adhesive are attached. (b) When the device is brought into contact with a surface, the object presses triggers and causes the arms to collapse. This action allows the film to conform to the object. (c) Forces and moments can now be applied through the frame body and transmitted to the object.

also necessary to allow the film to become slack to conform to an object after contact. To satisfy these two requirements, a bistable frame is implemented (see Fig. 7). Above the hinge is a preloaded spring with a large moment arm, and below the hinge is a strong tendon with negligible stretch and a second preloaded spring. The device has two energetically stable positions.

B. Curved Surface Gripper with Moment Ability

A limitation of the flexible curved surface gripper is its inability to apply moments. In certain pick-and-place operations, this may not cause issues; however, there are many cases in which a gripper is asked not only to lift, but also to rotate, an object. To meet this requirement, we present a curved surface gripper with moment application ability.

The frame of the device consists of a frame body and two arms; the arms are hinged at the extents of the frame body, again in a bistable fashion [see Fig. 8(a)]. Triggers extend proximally from each arm. When the device is brought lightly into contact with a surface, the triggers make contact and are pressed toward

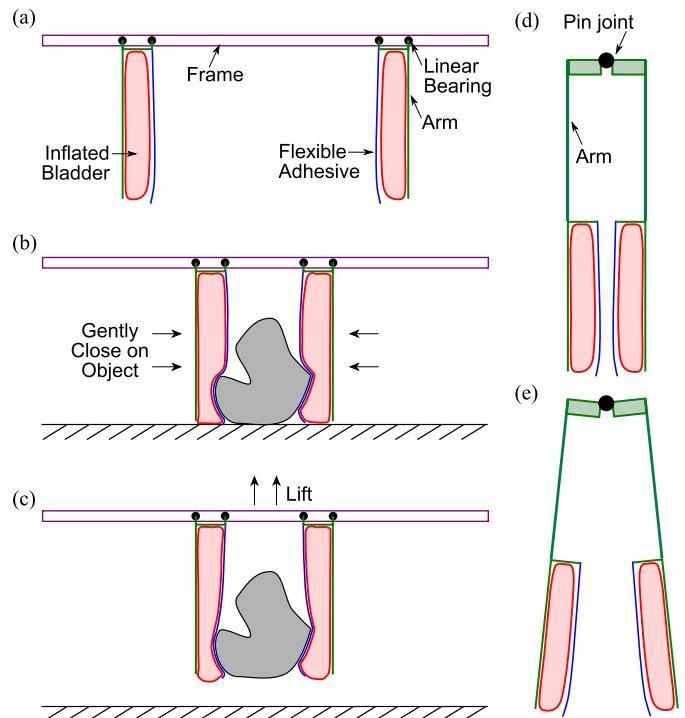


Fig. 9. (a) Lateral gripper consists of two arms extending perpendicularly from the frame. The two arms move on a linear bearing along the frame. On each arm is an inflated bladder, with a thin film of adhesive resting on the inner surface. (b) Two arms are brought in to close around an object of arbitrary shape. (c) Frame is lifted, and shear force from the adhesive lifts the object. (d) Alternative version of the gripper with a single pivot joint. (e) Gripper opens as the two arms pivot away from one another.

the frame body so that the arms collapse, allowing the film to conform to the object [see Fig. 8(b)]. However, because the film is attached to the rigid frame body at two points separated by a distance, the device can apply moments [see Fig. 8(c)]. The resultant of the shear forces provides the normal force for lifting the object and, when combined with a pressing normal force from the frame, it also enables the application of moments.

C. Lateral Gripper

The previous gripper designs focused on the problem of grasping a curved, convex object. While many everyday objects fall into this category (especially in the application of pick-and-place in manufacturing or packaging), the eventual goal of this paper is to lift any object that a human hand can lift. To create a gripper capable of grasping an object of a more arbitrary shape, we first note that if the object has concavity, we cannot guarantee the film will lay flat against it. We, therefore, may need a small amount of force to hold the adhesive on the surface. Second, we note that it is only the component of the shear in the vertical direction that lifts the object; therefore, if we may attain only a limited area of contact, it is best for this area to have a tangent in the vertical direction. With these considerations in mind, we present the lateral gripper [see Fig. 9(a)]. We implement a very compliant air bladder behind each adhesive film, to help guarantee the film makes contact with the surface, despite

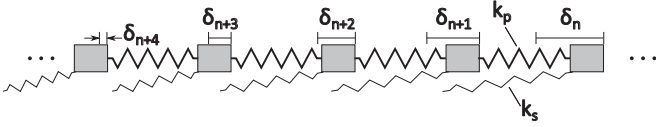


Fig. 10. Model of the polyamide film (horizontal springs) and silicone wedges (angled springs). When a load is applied, each node moves to the right.

irregularities. We also align the adhesive films vertically to maximize their contribution to the lifting force. Grasping is achieved by closing the gripper around an object, with just enough preload to deform the bladder [see Fig. 9(b)]. When lifting, the tension in the film applies a shear load through the adhesive.

The critical difference between this gripper and previous soft robotic grippers [20] that use load-controlled friction to grasp objects that are too large to envelop is that here the lifting force is not dependent on squeezing force. This is important for two reasons. First, it eliminates the need for sensing and controlling the squeezing force, because a single, predefined very light preload can be used regardless of object size, weight, or fragility. Second, soft grippers based on load-controlled friction cannot easily lift heavy objects because a large normal force cannot be produced with a very compliant gripper, whereas this gripper is capable of lifting objects with a mass of over 3 kg using only 5 cm² of contact area.

IV. MODELS

In this section, we present models of the adhesive film and of the grippers. The model for the simple curved surface gripper predicts load capability at a range of pull-off angles based on the shape of the object. The next model, for the gripper with moment ability, predicts the total load a gripper can provide, given a curvature. The final model predicts the lifting capability of the lateral gripper based on the geometry of the object. The models consider the characteristics of the surface as a parameter.

A. Film Shear Stress Model

In previous work [14], we considered the film to be inextensible, resulting in a constant shear stress across its length at the interface with the object. This model matched well with data, not because the film is truly inextensible, but because during stretch local slippage redistributes shear stresses. Here, we present a more accurate model that considers both stretch and slip, while assuming stretch is small enough that the film does not deform out of plane. Further, we assume that there are minimal internal varied preload forces within the film, because the bistable frame ensures that the spacing of the wedges is equal as the film is applied to a surface.

As a starting point, to understand how the load is distributed across the interface between the adhesive film and the object, we discretize the adhesive film into a number of nodes. A silicone wedge, or small group of wedges, has a stiffness k_s and is supported by segments of film with stiffness k_p (see Fig. 10). Performing a force balance on each node allows us to express the displacement of the n th node δ_n in terms of the two previous

displacements δ_{n-1} and δ_{n-2}

$$\delta_n = \frac{2k_p + k_s}{k_p} \delta_{n-1} - \delta_{n-2}. \quad (1)$$

Because (1) is a linear homogenous recurrence relation with constant coefficients, the solution can be written as

$$\begin{aligned} \delta_n = & C_1 \left(\frac{2k_p + k_s}{2k_p} + \sqrt{\left(\frac{2k_p + k_s}{2k_p} \right)^2 - 1} \right)^n \\ & + C_2 \left(\frac{2k_p + k_s}{2k_p} - \sqrt{\left(\frac{2k_p + k_s}{2k_p} \right)^2 - 1} \right)^n \end{aligned} \quad (2)$$

where C_1 and C_2 are constants determined by boundary conditions. Using the maximum stretch, found at the first wedge (20 μm), as well as the stiffness of the polyamide film and a polydimethylsiloxane (PDMS) silicone wedge, (2) predicts a maximum force of roughly 8 N, spread over approximately the first 120 wedges, or 12 mm. Because of the large ratio of k_p to k_s , the magnitude of the shear load on each wedge decreases approximately linearly.

This calculation leads to an apparent incongruity: If only 8 N can be applied before film stretch leads to the first wedge being overloaded, how can the film support 80 N? The answer to this question lies in an interesting property of the adhesive: dynamic adhesion [16]. Even after wedges begin to slip on the surface, the adhesion, and thus the adhesion-controlled friction, remain close to the static case, even slightly increasing up to a slip rate of 10 mm/s [21]. A similar behavior is seen in the gecko [21]. Therefore, as suggested by the above model, with a light load, a linear decrease in shear stress is seen across a small section of the film at its interface with the object [see Fig. 11(a)], while at larger loads, once slip begins, a uniform shear stress is seen across the entire slipped region [see Fig. 11(b) and (c)]. In order to determine the maximum shear load that a film can support, only a model of the slipped region is necessary; at maximum load before failure, all but the very last wedge will have slipped.

We seek to build a model that describes both stretching and slipping of the adhesive at a peel angle of zero (pulling along the surface tangent). Most previous models of adhesion and peeling have leveraged an energy balance following the method of the Kendall peel model [22]. This method has been used in modeling gecko adhesives, especially when determining the maximum load of the filmlike spatula [23]–[25]. These studies do not consider slipping; however, a more recent work [26] adds this term. This paper models the failure of gecko spatulae considering the work done during a slip, but not the effect of stretch, meaning a slip occurs only during failure. Tape peeling models that incorporate stretch and slip are quite relevant [27], [28], however, they do not consider the cases where the peel angle is zero, or when the slip zone is much larger than the thickness of the tape, as in the present case.

In creating a model capable of including both slipping and stretching of a film while pulled along a surface, we assume pulling along a flat surface for simplicity. In the gripper application, we pull along a gently curved surface; however, the curve simply adds a slight normal preload to the film (see

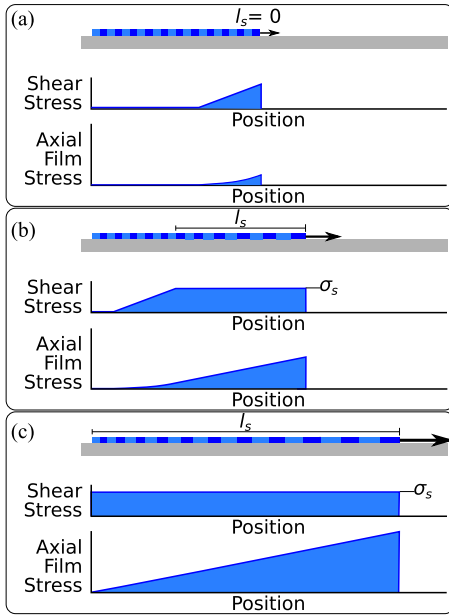


Fig. 11. (a) At light loads, the adhesive does not slip, resulting in negligible stretch; the shear stress at the interface with the object drops off linearly, as predicted in (2), and the internal axial film stress has a second-order relationship with position along the film (simply the integral of the shear stress). (b) At a larger load, the film stretches over a length l_s , resulting in a uniform shear stress σ_s or the stress required to slip, in this region. (c) At maximum load, the entire film is stretched, and there is a uniform shear stress (and linearly increasing axial film stress) across the entire length.

Section III-A1), which adds to the adhesion and slightly increases total normal force but is assumed to have a negligible effect on the overall behavior.

We begin by noting that an energy balance is not necessary in our case, because we are not actually peeling, but only sliding. No new surfaces are created, so there is not an energy term due to the separation of the film from the adherend surface. We can, therefore, define force per unit length required to slip the film along the surface as simply the shear stress limit (assumed to be equal to the shear stress at the interface while sliding [21]) σ_s times the film width b . Thus, for a given length of slipped film l_s , the slipping force F can be written as follows:

$$F = \sigma_s b l_s. \quad (3)$$

We can now predict the shear force that a length of slipped film can support. It is interesting to note that the predicted force when the entire film has stretched is identical to that predicted if the film is considered inextensible, as assumed in previous work [14]. Finally, it is useful to predict the amount of stretch d of the film by integrating the film strain across the slipped region

$$d = \frac{F^2}{2Eb^2t\sigma_s} \quad (4)$$

where E and t are Young's modulus and the thickness of the film, respectively.

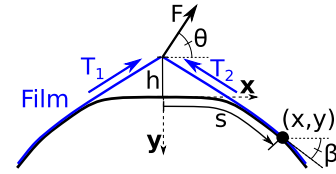


Fig. 12. Geometry upon which the varying curvature model is based.

B. Simple Curved Surface Gripper Model

In this section, we develop a model for the load capacity of the simple curved surface gripper. A number of assumptions are made in this model. First, the object is assumed to be of a uniform material, with uniform surface texture and is symmetric. The object is modeled as having its center of mass at its centroid,² and to have a radius of curvature for the surface extending into the page that is large enough that the film makes full contact across its width. The only force from the film that is considered is the shear force; the very small normal adhesion force at the peel zone (less than 0.25 N in practical examples) is neglected so that the film can be modeled as leaving the surface along the tangent. We also neglect the small compressive normal force due to the curvature of the film (see Section III-A1).

The model is based on the geometry shown in Fig. 12. The model uses the total length of film L , the distance from the object to the apex of the gripper (where the two films meet) h , and the angle between the load (F) and the horizontal θ . The model seeks to predict the total force knowing only L , h , θ , and the shape of the object.

We describe the two-dimensional shape of an object using the length along the curve s and direction of the curve β , which are related by a function C

$$\beta = C(s). \quad (5)$$

Then, the x and y coordinates at s are found as

$$x = \int_0^s t \cos C(t) dt \quad (6)$$

$$y = \int_0^s t \sin C(t) dt. \quad (7)$$

Now, we define a coordinate (x, y) , where the film leaves the surface, and determine it as the point where

$$\beta = \text{atan}\left(\frac{h+y}{x}\right). \quad (8)$$

We set the horizontal and vertical distance from the apex to this point as X and $Y + h$, respectively. For the case when $\text{atan}((Y + h)/X) < \theta \leq \pi/2$, both sides of the film will be in tension, and the maximum force F can be calculated based on the film tensions (T_1 and T_2) and the value of β at (x, y) , which

²This assumption allows us to equate the tension in the two films for simplicity; however, asymmetry is readily handled by the gripper with unequal film tension.

is the film angle α

$$F \cos \theta = T_1 \cos \alpha - T_2 \cos \alpha \quad (9)$$

$$F \sin \theta = T_1 \sin \alpha + T_2 \sin \alpha \quad (10)$$

where T_1 reaches the shear force limit T_{\max} . Solving for F and substituting for α yields

$$F = \frac{2T_{\max}X(Y+h)}{((Y+h)\cos(\theta) + X\sin(\theta))\sqrt{X^2 + (Y+h)^2}}. \quad (11)$$

Finally, T_{\max} is $\sigma_s b(L - \sqrt{X^2 + (Y+h)^2})$. With (11), we are able to predict the maximum force that can be applied to the curved surface gripper, given a loading angle and a parametric equation describing a convex surface. We note that for the case where $\theta = \pi/2$, we have

$$F = 2\sigma_s b(L - \sqrt{X^2 + (Y+h)^2}) \frac{Y+h}{\sqrt{X^2 + (Y+h)^2}} \quad (12)$$

which is simply the product of the shear stress limit ($2\sigma_s b$), the area in contact ($L - \sqrt{X^2 + (Y+h)^2}$), and the proportion of the film tension in the vertical direction ($\frac{Y+h}{\sqrt{X^2 + (Y+h)^2}}$). We can see that larger lifting forces can be applied to surfaces that have high radii of curvature near the center of the gripper, such that the distance to the point where the film leaves the surface (x, y) is smaller. This increases both the area of contact as well as the proportion of the tension in the vertical direction.

Finally, for the case when $\text{atan}((Y+h)/X) \geq \theta > 0$, only one side of the film will be in tension. If a spacer is used under the apex to define h , then the area in contact does not change with θ . Therefore, the maximum force for this set of loading angles is simply

$$F = 2\sigma_s b. \quad (13)$$

With this model, we are able to predict the maximum force that the simple curved surface gripper can apply, and explore how this force varies as the shape of the object, the angle of the load, the length of the film, and the height of the offset change.

C. Gripper with Moment Ability Model

In the previous section, we developed a model to predict the maximum load that can hang from a simple curved surface gripper. However, the gripper with moment ability can also apply a torque to an object, and we therefore wish to create a model to predict this moment capability. We make the same assumptions used in Section IV-B, and now also assume that the forces from the frame on the body, C_1 and C_2 , are compressive, and the forces from the film on the body, T_1 and T_2 , are tensile (see Fig. 13). We assume a constant curvature object in this model. Further, we assume that the film does not stretch enough to greatly change the angle of the frame body with respect to the object. However, we note that even an infinitesimal stretch results in the upper contact point of the frame body losing contact, and thus we assume $C_2 = 0$.

We next note that the sum of the moments about the center of the object yields that $T_1 = T_2$. After taking the sum of the

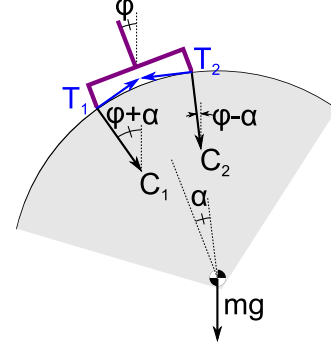


Fig. 13. Free body diagram of the object.

forces in both the x and y directions, we find

$$mg = \frac{2T \sin^2(\alpha)}{\sin(\phi + \alpha)} \quad (14)$$

where ϕ is the angle between the frame body and the vertical, and α is the angle defined by three points: The center of the frame body, the center of the object, and a contact point between the frame body and the object. Further, the maximum value of the object weight mg is found by setting T equal to T_{\max} , as was done above. Note that in the case in which $\phi = 0$, we find the same result as for the curved surface gripper at $\theta = \pi/2$ (12), because there are no applied moments ($C_1 = C_2 = 0$).

Note that (14) is valid only if $(\phi + \alpha)$ is less than π so that the denominator is positive, otherwise one side of the frame contact point can wrap around the object from underneath to support the external load. In other words, there is no adhesive film tension T_1 and T_2 ; only the compressive forces C_1 and C_2 are present for this scenario. The load capability is only dependent on the frame strength.

When $(\phi + \alpha)$ is less than $\pi/2$, $\sin(\alpha)$ increases faster than $\sin(\phi + \alpha)$ as α increases. Thus, the right-hand side of (14) increases monotonically as α increases. When $(\phi + \alpha)$ is between $\pi/2$ and π , $\sin(\phi + \alpha)$ decreases as α increases. Thus, the right-hand side of (14) still increases monotonically as α increases. Therefore, before the frame wraps around the object and assuming a fixed size of adhesive, it is always desirable to have a large α for maximum load capability in any loading direction.

We are now able to predict the maximum force the gripper with moment ability can apply to an object, knowing the geometry of the gripper and object, as well as the angle of load and shear stress limit.

D. Lateral Gripper Model

The final model predicts the lifting capacity for the lateral gripper, described in Section III-C. The model assumes that the shape and surface characteristics of the object to be grasped are known. As in the previous models, we assume the maximum shear force is proportional to the area in contact when the gripper is under load. Also as above, normal adhesion at the peel zone is considered to be small, as is any normal compressive force due to the curvature of the film.

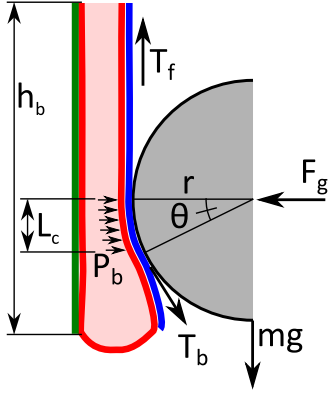


Fig. 14. Force balance used for determining area of adhesive film in contact with an object in the lateral gripper model.

To build a simple model with these assumptions, we need only to determine the amount of area the film has in contact with a given object. Because the film is assumed to extend vertically from the object (see Fig. 14), all of the tension in the film is due to the weight of the object. This is in contrast to the curved surface gripper model, in which there is a horizontal component of tension that is internal. To determine the area of film in contact with a convex object, we use a force balance, as shown in Fig. 14. The force applied to the object by one side of the gripper F_g must balance the force that the bladder applies to the object. This force has two components: The pressure in the bladder P_b multiplied by the area of adhesive in contact A_a and the horizontal component of the tension in the bladder wall T_b . The area of the adhesive A_a can be written as $L_c W$, where L_c is the length of the adhesive contact, and W is the width of the gripper, measured into the page. We then write

$$F_g = P_b L_c W + 2TW \sin \theta. \quad (15)$$

For small angles, $\sin \theta \approx L_c/2r$. The tension in the bladder wall is related to the pressure and the height of the bladder h_b

$$h_b P_b = T_b + F_g/W. \quad (16)$$

The shear load F_s is

$$F_s = \sigma_s A_a. \quad (17)$$

Rearranging (15) and (16), we obtain

$$F_s = \sigma_s W \frac{F_g r}{P_b W r + P_b h_b W - F_g}. \quad (18)$$

We can now predict the weight of a cylindrical object that the lateral gripper can lift, assuming we know the geometry of the object and the shear stress limit.

V. RESULTS

We present tests to validate the models in the previous section. Additional tests evaluate the performance of the adhesive film on a nonsmooth surface. We also present results of grasping tasks with the simple curved surface gripper and the lateral gripper, demonstrating some of the capabilities of shear-activated grippers.

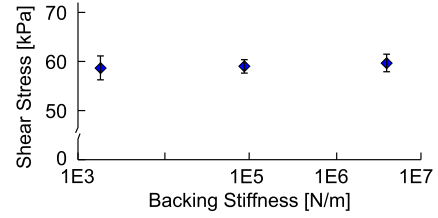


Fig. 15. Data showing the relationship between the maximum shear stress and the elastic modulus of the backing layer for vinyl (1.8E3 N/m), polyamide (8.9E4 N/m), and stainless steel (4.1E6 N/m). Error bars show one standard deviation.

A. Model Validation

Before considering each of the gripper models, we address the film stretch and shear stress model.

1) *Film Shear Stress Model Results:* The film shear stress model predicts a proportional relationship between the applied force and the length of the film that has stretched and slipped (3). Therefore, the model predicts that once the entire film has slipped, the total force is the same regardless of film stiffness. Note that the assumptions of the model preclude very soft films. We tested this prediction by finding the maximum shear stress from films with three different stiffnesses: vinyl (1.8E3 N/m), polyamide (8.9E4 N/m), and stainless steel (4.1E6 N/m). The films were tested on a smooth plastic surface, and maximum force was recorded with a Mark-10 M4-50 digital pull-scale, with a 3-kHz sampling rate and accuracy of 0.2% full scale. No external preload was applied to the samples, besides the weight of the sample itself (less than 0.01 N). Each sample was tested four times. As seen in Fig. 15, all three films show similar performance; using the averages and standard deviations from the measurements, we are able to say with confidence of 95% ($p \leq 0.05$) that none of the maximum shear stresses varies by more than 5 kPa across the three orders of magnitude of stiffness. These data also show that the shear stress is roughly uniform across the film, because the total stress for the entire film is equivalent to the shear stress limit of the film (roughly 60 kPa); if any section of the film were loaded below its capacity, the total stress would be lower than the shear stress limit.

The model also suggests that when a film stretches and continues to support a shear load in the slipped regions, the total displacement should be directly related to the square of the force applied (4). To test the model, we measured the total displacement of a thin adhesive film and the force applied along the surface while stretch and slip occurred. We again measured with the Mark-10 M4-50 digital pull-scale and applied no external preload besides the weight of the sample. We tested the behavior on a gently curved, slightly textured surface. The results from a test are shown in Fig. 16. Also plotted is the model based on (4), with $E = 2$ MPa, $b = 7$ mm, $t = 0.2$ mm, and $\sigma_s = 20$ kPa. E , b , and t are measured, and σ_s is calculated using (3), with measured F , b , and l_s .

2) *Curved Surface Gripper Model Results:* To evaluate the curved surface gripper model, we first loaded the gripper in a direction perpendicular to the surface with a constant offset height while varying the radius of curvature of the surface. Next,

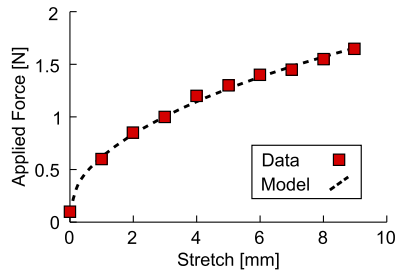


Fig. 16. Data showing the relationship between the applied force and the total displacement of the leading edge of a stretching adhesive film, with the model based on (4).

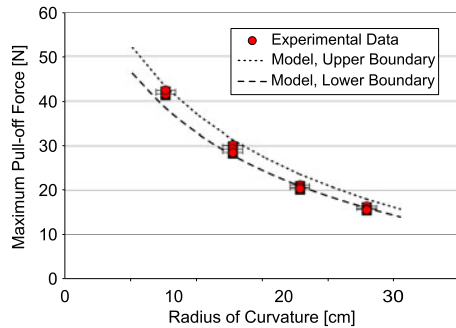


Fig. 17. Maximum pull-off force versus radius of curvature. Model, based on (12), is shown in dotted lines, with upper and lower boundaries determined using maximum and minimum values of expected shear stress limit. Error bars show uncertainty in radius of curvature.

we kept the radius of curvature constant and varied the offset height. Third, we again varied offset height, but on a surface with two distinct radii of curvature. Finally, we kept both the radius of curvature and the offset height constant and varied the loading angle.

We laser machined a fixture with five curved slots, each at a different radius of curvature from 7 to 28 cm. A 2-mm thick sheet of nylon was bent and fit into one of the curved slots for each test. A curved surface gripper (two opposed adhesive films) was placed on the curved nylon sheet with a small spacer that controlled the initial offset height to the load tendon (see Fig. 4). The gripper was loaded with the central load tendon at a rate of roughly 3 N/s until failure. The final offset height, h (slightly larger than initial offset height due to film stretch) was recorded with a high-speed camera at 400 fps and analyzed in MATLAB. Either three or four tests were performed for each curvature.

The results of the tests and model from (12) are shown in Fig. 17. Parameters for the model are film length, $L = 8$ cm, film width, $b = 2.2$ cm, and shear stress limit, $\sigma_s = 64 - 82$ kPa (measured range), and X and Y are determined from the geometry of each setup. For the radii tested, both the model and the data show that the expected load decreases with increasing radius of curvature. The upper and lower limits were determined using identical geometry but with the maximum and minimum expected values of the shear stress limit. The model shows an asymptote at zero force as the radius of curvature approaches infinity. In practice, a small amount of normal adhesion exists

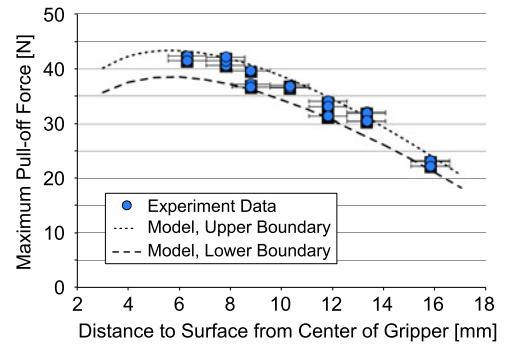


Fig. 18. Maximum pull-off force versus offset height h for the load tendon. Model, based on (12), is shown in dotted lines, with upper and lower boundaries determined using the maximum and minimum values of the expected shear stress limit. Error bars show uncertainty in offset height.

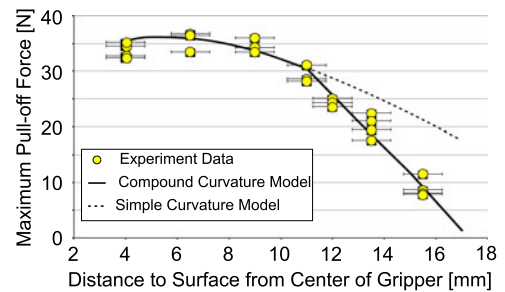


Fig. 19. Maximum pull-off force versus offset height h for an object with two radii of curvature. Model, based on (12), is shown in solid lines. Also shown, with a dotted line, is the model if only the initial curvature is considered. Error bars show uncertainty in offset height.

at the peel zone, so nonzero loads can be supported even on flat surfaces. Another inaccuracy of the model is the prediction that the force continues to increase as the radius of curvature decreases. This effect results from the fact that the model does not take into account the total available surface area of the object. Therefore, in reality, the total area available to support shear load begins to decrease at a certain small radius of curvature, resulting in a decrease in total shear load capability.

The second test was performed while the radius of curvature was fixed at 12.5 cm, and the offset height was varied from approximately 6 to 16 mm. The results of the tests and model for varied offset height are shown in Fig. 18. The data and model both show a generally decreasing maximum load for increasing offset height. The model, however, predicts a peak load at an offset height of roughly 6 mm. As the offset height decreases further, the proportion of the tension in the vertical direction to horizontal direction decreases more quickly than the contact area increases (12). The data do not extend to offset values lower than 6 mm because the current film stretches enough to make it infeasible to test these offset values.

In the third test, we again varied the offset height, but on a surface with two different radii of curvature. The surface has a radius of curvature of roughly 12.5 cm in the center section and 30 cm on either side. Results are shown in Fig. 19, along with the model from Section IV-B. Because of the step change in

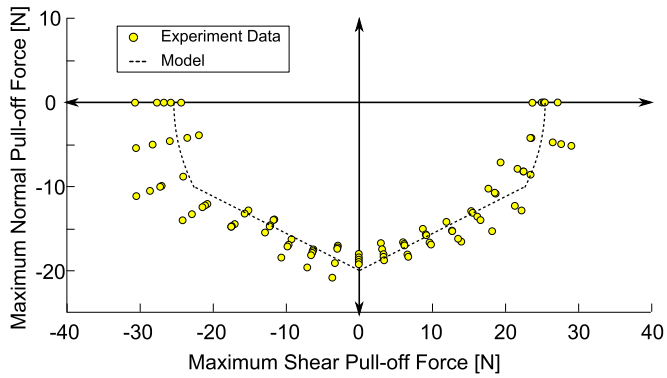


Fig. 20. Maximum force a curved surface gripper can apply at different loading angles, as well as model from (11).

the curvature of the surface, the model predicts a nonsmooth pull-off force as the offset height varies. While the gripper is in contact with the smaller radius of curvature section, the pull-off force is high; once the offset height increases such that the gripper only contacts the larger radius of curvature section, the pull-off force drops quickly.

We additionally tested the performance of the curved surface gripper at 19 different pull-off angles ranging from pure shear in both directions (tangent to the surface) to pure normal (perpendicular to the surface). At least four data points were taken at each angle. The radius of curvature and offset height were fixed at 12.5 cm and 10 mm, respectively, and the adhesive films had length of 6 cm and width of 2 cm. The results of the tests are shown in Fig. 20, along with the model described in Section IV-B. The model predicts two lines, reflected about the y axis, as described by (12). At loading angles close to pure shear, one of the tendons will become slack, and the model predicts a curved section, described by (13).

3) *Gripper with Moment Ability Model Results:* A gripper with moment ability, as described in Section IV-C, with adhesive films of length 4 cm and width 2.5 cm, was set on a polyvinyl chloride (PVC) cylindrical surface with radius of curvature of 5.2 cm. The gripper frame contact points are spaced apart by 5.2 cm, and the angle α is 30° . The set up was on a horizontal, low-friction table. The gripper was fixed to the table, and the object was loaded at a prescribed angle with respect to the gripper's central axis through the object's center of mass. A digital pull-scale measured the load until the gripper failed. At least five trials were performed at each angle. The results are shown in Fig. 21, along with the model from (14). As predicted by (14), we see a sharp decrease in load capacity as the angle ϕ increases initially, then a plateau as ϕ continues to increase, due to the $(1/\sin \phi)$ term.

4) *Lateral Gripper Model Results:* We tested the maximum load the lateral gripper could apply to four different objects: A cylinder with radius 5.7 cm, a cylinder with radius 1.7 cm, a rectangular prism with square cross section and side length 4 cm, and a rectangular prism with square cross section and side length 1.9 cm. All surfaces were covered in paper to give a uniform texture, resulting in a shear stress limit σ_s of roughly 2.3 kPa. The gripper had a width W of 8.5 cm, a preload F_g of

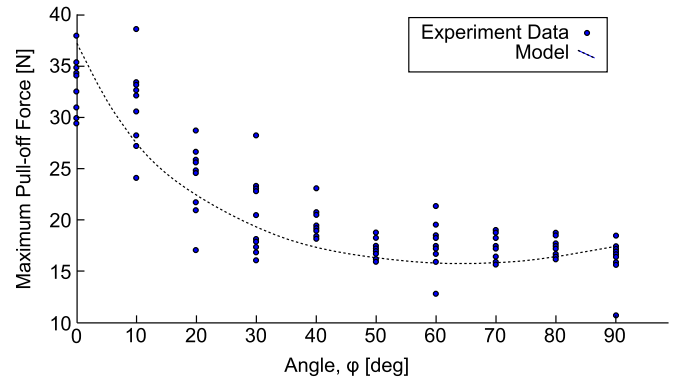


Fig. 21. Maximum pull-off force a gripper with moment ability can apply at different angles with respect to the vertical along with model from (14).

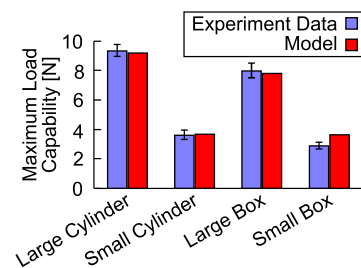


Fig. 22. Measured and predicted (18) maximum load capability for the lateral gripper on various shapes covered in paper.

0.75 N, a bladder height h_b of 15 cm, and an internal pressure P_b of 0.145 kPa. Each object was tested at least five times. The results of the tests as well the predicted performance from the model (18) are shown in Fig. 22. Larger objects are predicted to have higher maximum loads because more surface area is in contact with the adhesive.

B. Performance on Various Surfaces

1) *Performance on Varied Textures:* We ran a series of tests in which we dictated a range of pressing preloads on the back of both the adhesive and a textured sheet of silicone rubber foam (a material that might be used on a robotic finger), while measuring the maximum shear load. We repeated the tests on various surfaces ranging from microrough, such as paper, to smooth, such as varnished wood and acrylic. Fig. 23 shows the results. There are a few notable effects. First, for both the adhesive and the textured rubber, all surfaces show a positive relationship between shear stress and normal preload force, as one would expect from a frictional behavior. This relationship between preload and shear stress has a similar slope for all materials tested. However, for the adhesive on smoother surfaces, we see a higher shear stress at zero normal preload. This effect is what allows grasping without squeezing for smooth surfaces: The application of a shear stress results in adhesion which in turn results in adhesion-controlled friction. As surface roughness increases, we are required to increase the squeezing force to achieve similar shear stresses. At a certain level of roughness (e.g., paper), a large normal pressure (beyond the range tested)

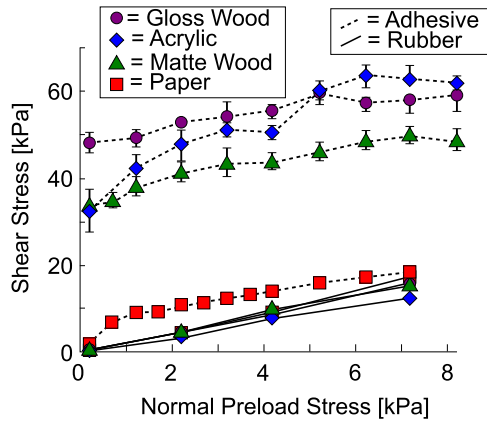


Fig. 23. Data from tests relating the maximum shear stress to preload normal force for adhesive and textured rubber on surfaces with varied roughness. Rougher surfaces require higher preload to achieve large shear stress values.

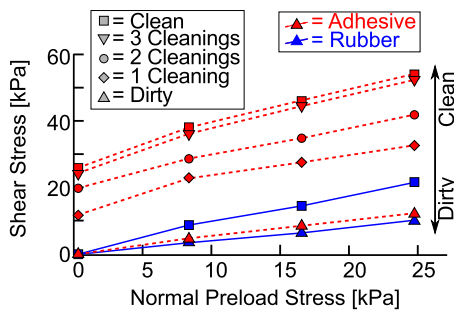


Fig. 24. Data from tests relating the maximum shear adhesive stress to preload normal force for both adhesive and textured rubber with varied levels of contamination. Dirty adhesive performs roughly the same as dirty rubber, but with cleaning regains full performance.

would be needed to match the shear stress available on smooth surfaces such as varnished wood. Notably, the performance of the adhesive on the roughest surface tested, paper, is similar to that of textured rubber on all surfaces. In summary, friction has two components, adhesion controlled and load controlled, and we see the adhesion-controlled portion as an offset in the positive y -direction.

2) *Performance with Varied Contamination*: We also tested the effect of contamination on the adhesive, as compared to textured silicone rubber foam. Samples with area 6 cm^2 of adhesive and textured rubber were tested on a matte finish wood surface in shear with varied normal preloads. After completing tests with clean samples, the adhesive and the textured rubber were completely covered with talc powder. The excess was brushed off. The samples were then retested. A series of cleaning cycles were then completed for the adhesive sample. The sample was set on a piece of 3M 3850 heavy duty packing tape and pressed with 2 N of normal force. The sample was retested, then cleaned a second time. This process was repeated one more time. The results are shown in Fig. 24. The adhesive, when fully contaminated, performs roughly the same as a contaminated textured PDMS sample. This is because the adhesion-controlled friction is reduced with contamination, but the load-controlled friction

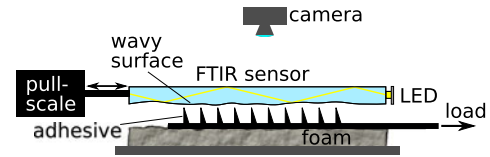


Fig. 25. Experimental setup for testing the performance of adhesive film on wavy surfaces while recording video of the surface illuminated with FTIR.

remains. However, with three simple cleaning cycles, the adhesive returns to full performance.

3) *Performance on Millimeter-Scale Roughness*: We tested the performance of the adhesive film on marbled glass with undulations with depths of roughly $500 \mu\text{m}$ and spacing of roughly 10 mm , to evaluate the effect of millimeter-scale surface variations, and we compared it to the performance of film coated with flat PDMS. At this scale, the wedges (roughly $80\text{-}\mu\text{m}$ tall) are not tall enough to accommodate the surface undulations; therefore, the adhesive film must conform. The wedges are able to pull the flexible film down into the contours of the surface, as shown schematically in Fig. 3. To quantify this effect, we created a frustrated total internal reflection (FTIR) test setup, as shown in Fig. 25. An LED shines light into the end of a section of marbled glass, and a camera observes the glass from above. The adhesive film is placed below the glass on a piece of foam. The film is loaded while a digital pull-scale measures the reaction force required to prevent the glass from moving.

Images from the camera, after thresholding and converting to black and white, are shown in Fig. 26(a). White areas in the screenshots represent areas where the adhesive is in contact with the glass (due to the contact, refracted light is able to escape the glass in these areas). The images show that as the applied shear load increases, the contact area increases for the fibrillar adhesive but not for the flat PDMS. This result is shown in Fig. 27, on a plot of contact area versus shear load. While the flat PDMS performs as well or better than the fibrillar adhesive at low loads, when the shear load increases, the fibrillar adhesive greatly increases contact area and shear load ability. A side view of the adhesive film on the marbled glass shows how the wedges pull the film down into the valley of the glass as more shear load is applied [see Fig. 26(b)].

C. Grasping Task Results

Finally, we performed a series of grasping tasks, some with the simple curved surface grippers and others with the lateral gripper. The results of the tests demonstrating some capabilities of shear-activated grippers are described ahead.

1) *Simple Curved Surface Gripper Tasks*: We built a curved surface gripper with a bistable frame and mounted it on an Adept 5-DOF robotic arm. The robot touched the gripper to an object to grip, and pulled a cable attached to the two outer tendons to release (visible in Fig. 1).

We placed four objects sequentially in the workspace of the arm, and the robot picked, moved, and placed each object (see Fig. 28). The 3.5-kg tubing is an example of the gripper's ability to lift and move heavy objects, while the water jug and basketball

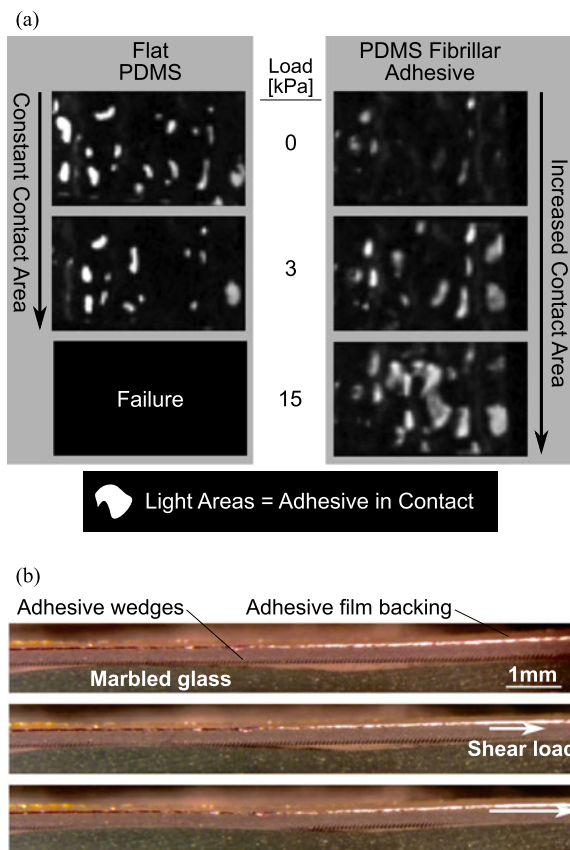


Fig. 26. (a) FTIR images of both flat PDMS (left) and fibrillar adhesive (right) when loaded in shear on a wavy surface. At higher shear loads, the adhesive has more contact with the surface, increasing its gripping ability. (b) *Top*: Micrograph of a side view of the adhesive film on marbled glass. *Middle*: As shear load is applied to the film, wedges in contact lay over, pulling the neighboring wedges and film into better contact. *Bottom*: As shear load increases, the film is pulled down into the valley of the marbled glass.

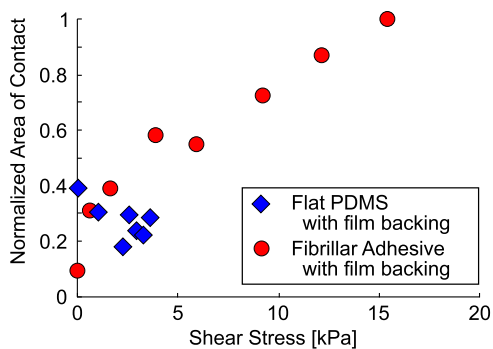


Fig. 27. Data showing the relationship between the contact area and the shear load and for both flat PDMS and fibrillar adhesive.

are examples of grasping a large object without reaching around the sides of an object. As a final test, the gripper lifted a plastic bag filled with water, in order to demonstrate the ability to grasp an unconventional object without squeezing (see video in supplementary material).

We tested the speed of the curved surface gripper by catching a thrown ball (see Fig. 29). Because the rate at which PDMS can



Fig. 28. Grasping tasks with a curved surface gripper implemented on a robotic arm. The gripper is shown lifting (clockwise from upper left): packing tape, 3.5-kg PVC tubing, empty 5-gal water jug, and a regulation basketball.



Fig. 29. Curved surface gripper passively catching a ball thrown at it.

bond to or peel from a surface is limited [29], it is imperative to have many fibrillar contacts bonding in parallel. This allows for a bond to form considerably faster than would be possible with flat PDMS [17]. Because the gripper works passively, it can be very light; no high-power actuator is needed, nor any sensing. A light gripper means that the device can rebound with the ball after initial contact, reducing the maximum shear stress [30].

2) *Lateral Gripper Grasping Tasks*: To test the lateral gripper in a practical setting, we picked up 23 objects of various shapes, sizes, textures, and weights selected from an online distributor and placed them into a cardboard box. The objects included a shower pouf, a 1-kg bag of chia seeds, a basketball net, a triangular box, and a bottle of chocolate syrup. This task is shown in the video (i.e., Supplementary material). Further, we tested the gripper with objects that are difficult for traditional grippers (see Fig. 30). We show grasping of large and small items, ranging from 1 m to 1 mm in diameter, as well as heavy (3.4 kg) to delicate. No modifications were made to the gripper. In all cases, the preload arose only from the weight of the arms. No sensing or active grasp control was required.

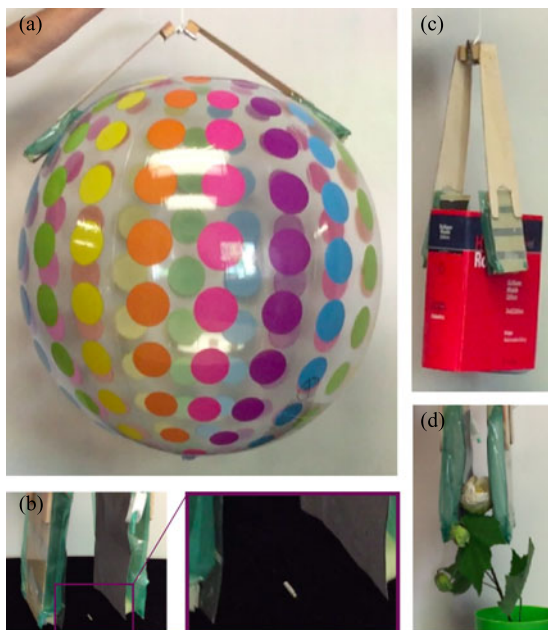


Fig. 30. Sampling of objects that the lateral shear gripper can lift. (a) 1-m diameter ball. (b) 1-mm diameter pin. Inset at right shows magnified view. (c) 3.4-kg book. (d) Flower. Note that the same preload, supplied only by the weight of the arms is used to lift both heavy and delicate objects.

VI. DISCUSSION

The majority of this paper has focused on what shear-activated grippers *can* accomplish; however, it is helpful to also discuss the limitations of the concept. The chief limitation stems from the performance of the adhesive material on nonideal surfaces. Such nonidealities include microroughness and contamination. While it is clear from Section V-B that nonideal surfaces decrease the performance of the adhesive substantially, we also see that in the worst case scenarios, the adhesive results in friction at the same level as a textured sheet of the same material. This is practically important because if one is considering implementing a shear-activated gripper using the adhesive material, these results suggest that in all cases tested the adhesive performs as well or better than the traditional textured rubber. This is because even when the adhesion-controlled friction is no longer functioning due to lack of adhesion to the surface, load-controlled friction still remains.

Another limitation of the proposed designs is for dextrous manipulation. For the most part, the designs are meant for pick-and-place operations, without complex repositioning of the object within the grasp. However, the concept of shear-activated grippers is not incompatible with dextrous manipulation. The design of grippers with such capabilities might involve a modified adhesive material that allows slip in certain directions or under certain conditions. Analogous concepts are explored in the Velvet Fingers gripper, however, using a moving surface to approximate varied friction [31].

VII. CONCLUSION

In this paper, we explored the concept of shear-activated grippers. Unlike traditional grippers, which use load-controlled fric-

tion forces created by normal forces to grasp objects that are too large to envelop, shear-activated grippers rely on a special adhesive material that creates adhesion when loaded in the shear direction that in turn results in adhesion-controlled friction. This means that the lifting force does not scale with the squeezing force, but rather with the area of the adhesive material in contact. We discussed the mechanics behind this material and introduced three gripper designs based on the concept.

- 1) *Simple curved gripper*: Shows the ability to lift objects larger than itself without requiring a squeezing force.
- 2) *Curved gripper with moment ability*: Adds the capability to apply moments to the object.
- 3) *Lateral gripper*: Adds the ability to lift objects with concavity.

We derived models of a thin film of the adhesive material, as well as models for each of the three grippers. We showed results validating these models, as well as results showing performance of the material on nonsmooth surfaces. Finally, we demonstrated the grippers in practical pick-and-place applications.

Future research will seek to answer questions such as: Can the adhesive be optimized to achieve peak performance on a specific surface (if the user knows that only one type of surface will be grasped)? Can electrostatic attraction be used to bring the adhesive into contact instead of the mechanisms presented in this paper? And how can dextrous manipulation be achieved with a shear-activated gripper?

ACKNOWLEDGMENT

The authors would like to thank G. H. Hawkes, Department of Mathematics, University of California Davis, for help with mathematical modeling.

REFERENCES

- [1] D. Prattichizzo and J. C. Trinkle, "Grasping," in *Springer Handbook of Robotics*. Berlin, Germany: Springer-Verlag, 2008, pp. 671–700.
- [2] M. Rakic, "The Belgrade Hand Prosthesis," *Proc. Inst. Mech. Eng.*, vol. 183, pp. 1968–69, 1969.
- [3] J. K. Salisbury and J. J. Craig, "Articulated hands force control and kinematic issues," *Int. J. Robot. Res.*, vol. 1, no. 1, pp. 4–17, 1982.
- [4] S. Jacobsen, E. Iversen, D. Knutti, R. Johnson, and K. Biggers, "Design of the Utah/MIT dextrous hand," in *Proc. IEEE Int. Conf. Robot. Autom.* IEEE, 1986, vol. 3, pp. 1520–1532.
- [5] M. G. Catalano, G. Grioli, A. Serio, E. Farnioli, C. Piazza, and A. Bicchi, "Adaptive synergies for a humanoid robot hand," in *Proc. Int. Conf. Humanoids Robots*, 2012, pp. 7–14.
- [6] F. Lotti, P. Tiezzi, G. Vassura, L. Biagiotti, G. Palli, and C. Melchiorri, "Development of UB hand 3: Early results," in *Proc. IEEE Int. Conf. Robot. Autom.* IEEE, 2005, pp. 4488–4493.
- [7] A. M. Dollar and R. D. Howe, "Joint coupling design of underactuated grippers," in *Proc. ASME 2006 Int. Des. Eng. Tech. Conf.* American Society of Mechanical Engineers, 2006, pp. 903–911.
- [8] C. Melchiorri and M. Kaneko, "Robot hands," in *Springer Handbook of Robotics*. Berlin, Germany: Springer-Verlag, 2008, pp. 345–360.
- [9] L. Birglen, T. Lalibert, and C. Gosselin, *Underactuated Robotic Hands*. Berlin, Germany: Springer, 2007.
- [10] E. Brown *et al.*, "Universal robotic gripper based on the jamming of granular material," *Proc. Nat. Acad. Sci. USA*, vol. 107, no. 44, pp. 18809–18814, 2010.
- [11] S. Song, C. Majidi, and M. Sitti, "Geckogripper: A soft, inflatable robotic gripper using gecko-inspired elastomer micro-fiber adhesives," in *Proc. IEEE Int. Conf. Intell. Robots Syst.* IEEE, 2014, pp. 4624–4629.
- [12] G. J. Monkman, "Compliant robotic devices, and electroadhesion," *Robotica*, vol. 10, no. 02, pp. 183–185, 1992.

- [13] J. Shintake, S. Rosset, B. Schubert, D. Floreano, and H. Shea, "Versatile soft grippers with intrinsic electroadhesion based on multifunctional polymer actuators," *Adv. Mater.*, vol. 28, no. 2, pp. 231–238, 2016.
- [14] E. W. Hawkes, D. L. Christensen, A. K. Han, H. Jiang, and M. R. Cutkosky, "Grasping without squeezing: Shear adhesion gripper with fibrillar thin film," in *Proc. 2015 IEEE Int. Conf. Robot. Autom.* IEEE, 2015, pp. 2305–2312.
- [15] J. N. Israelachvili, *Intermolecular and Surface Forces*. New York, NY, USA: Academic, 2015.
- [16] A. Parness *et al.*, "A microfabricated wedge-shaped adhesive array displaying gecko-like dynamic adhesion, directionality and long lifetime," *J. Roy. Soc. Interface*, vol. 6, pp. 1223–1232, 2009.
- [17] D. Christensen, E. W. Hawkes, A. Suresh, and M. Cutkosky, "utugs: Enabling microrobots to deliver macro forces with controllable, bio-inspired adhesives," in *Proc. IEEE Int. Conf. Robot. Autom.*, 2014, pp. 4048–4055.
- [18] P. Day, E. V. Eason, N. Esparza, D. Christensen, and M. Cutkosky, "Micro-wedge machining for the manufacture of directional dry adhesives," *J. Micro Nano-Manuf.*, vol. 1, no. 1, 2013, Art. no. 011001.
- [19] S. A. Suresh, D. L. Christensen, E. W. Hawkes, and M. Cutkosky, "Surface and shape deposition manufacturing for the fabrication of a curved surface gripper," *J. Mech. Robot.*, vol. 7, no. 2, 2015, Art. no. 021005.
- [20] D. Rus and M. Tolley, "Design, fabrication and control of soft robots," *Nature*, vol. 7553, no. 521, pp. 467–475, 2015.
- [21] N. Gravish, M. Wilkinson, and K. Autumn, "Frictional and elastic energy in gecko adhesive detachment," *J. Roy. Soc. Interface*, vol. 5, no. 20, pp. 339–348, 2008.
- [22] K. Kendall, "Thin-film peeling—the elastic term," *J. Phys. D, Appl. Phys.*, vol. 8, no. 13, 1975, Art. no. 1449.
- [23] B. Persson and S. Gorb, "The effect of surface roughness on the adhesion of elastic plates with application to biological systems," *J. Chem. Phys.*, vol. 119, no. 21, pp. 11437–11444, 2003.
- [24] R. Spolenak, S. Gorb, H. Gao, and E. Arzt, "Effects of contact shape on the scaling of biological attachments," in *Proc. Roy. Soc. London A, Math., Phys. Eng.*, vol. 461, no. 2054, pp. 305–319, 2005.
- [25] G. Huber, S. N. Gorb, R. Spolenak, and E. Arzt, "Resolving the nanoscale adhesion of individual gecko spatulae by atomic force microscopy," *Biol. Lett.*, vol. 1, no. 1, pp. 2–4, 2005.
- [26] Y. Tian *et al.*, "Adhesion and friction in gecko toe attachment and detachment," *Proc. Nat. Acad. Sci. USA*, vol. 103, no. 51, pp. 19320–19325, 2006.
- [27] M. R. Begley, R. R. Collino, J. N. Israelachvili, and R. M. McMeeking, "Peeling of a tape with large deformations and frictional sliding," *J. Mech. Phys. Solids*, vol. 61, no. 5, pp. 1265–1279, 2013.
- [28] R. R. Collino, N. R. Philips, M. N. Rossol, R. M. McMeeking, and M. R. Begley, "Detachment of compliant films adhered to stiff substrates via Van der Waals interactions: Role of frictional sliding during peeling," *J. Roy. Soc. Interface*, vol. 11, no. 97, 2014, Art. no. 20140453.
- [29] B.-m. Z. Newby and M. K. Chaudhury, "Friction in adhesion," *Langmuir*, vol. 14, pp. 4865–4872, 1998.
- [30] E. W. Hawkes *et al.*, "Dynamic surface grasping with directional adhesion," in *Proc. IEEE Int. Conf. Intell. Robots Syst.* IEEE, 2013, pp. 5487–5493.
- [31] V. Tincani *et al.*, "Velvet fingers: A dexterous gripper with active surfaces," in *Proc. IEEE Int. Conf. Robot. Autom.* IEEE, 2012, pp. 1257–1263.

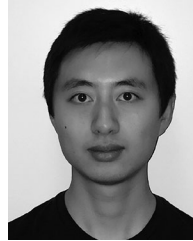


Elliot Wright Hawkes (M'11) received the A.B. degree with highest honors in mechanical engineering from Harvard University, Cambridge, MA, USA; the M.S. degree in mechanical engineering from Stanford University, Stanford, CA, USA; and the Ph.D. degree in mechanical engineering from Stanford University under the supervision of Prof. M. Cutkosky, in 2009, 2012, and 2015, respectively.

He is an Assistant Professor with the Department of Mechanical Engineering, University of California, Santa Barbara, Santa Barbara, CA, USA. His research

interests include compliant robot body design, mechanism design, nontraditional materials, artificial muscles, directional adhesion, and growing robots.

Dr. Hawkes was a Rhodes Scholar Finalist, a National Defense Science and Engineering Graduate Fellow, and a National Science Foundation Graduate Research Fellow.



Hao Jiang (S'13) received the B.S. degree in mechanical engineering from Beijing University of Aeronautics and Astronautics (BUAA or BeiHang), Beijing, China; the M.S. degree in mechanical engineering from Stanford University, Stanford, CA, USA, and the Ph.D. degree in mechanical engineering from Stanford University, in 2012, 2014, and 2017, respectively.

His research interests include applying bioinspired adhesive technology such as gecko adhesives and microspines to robotic gripper designs, as well as unmanned aerial vehicle (UAV) perching and sensing strategies with machine learning.

Mr. Jiang was the recipient of one ICRA Best Paper award and two IROS Best Papers awards as a coauthor.



David L. Christensen (S'12) received the Ph.D. degree in mechanical engineering from Stanford University, Stanford, CA, USA, in 2016 under the supervision of Prof. M. Cutkosky.

Before joining Stanford University, he was the Director of Research and Development with Valimet, Inc., Stockton, CA, USA, a manufacturer of micron-sized spherical metal powders used in applications including aerospace (solid rockets and turbine blades), metallic three-dimensional printing, automobile airbags, solar panels, and metallic pigments. He

worked on synthetic gecko adhesives, robotic sensors, and microrobotics with Prof. M. Cutkosky as well as the design of resonant microelectromechanical system (MEMS) sensors with Prof. T. Kenny. His research interests included mechatronics, MEMS, smart materials, and biomechanics during his time at Stanford University.

Dr. Christensen is an Accel Innovation Scholar, a Stanford program built to enable late-stage graduate students with the tools needed to undertake entrepreneurial endeavors, such as bringing their research out of the laboratory and into the world.



Amy K. Han (S'15) received the Bachelor's degree in mechanical engineering from Georgia Institute of Technology College of Engineering, Atlanta, GA, USA, and the Master's degree in mechanical engineering from Stanford University, Stanford, CA, USA, in 2012 and 2015, respectively. She is currently working toward the Ph.D. degree in mechanical engineering at Stanford University.

Her research interests include bioinspired robotics, electroactive polymers, and haptics.



Mark R. Cutkosky (M'92–F'12) received the Ph.D. degree in mechanical engineering from Carnegie Mellon University, Pittsburgh, PA, USA, in 1985.

He is the Fletcher Jones II Professor in mechanical engineering with Stanford University, Stanford, CA, USA. His research interests include robotic manipulation and tactile sensing, and the design and fabrication of biologically inspired systems. He has authored or coauthored extensively in these areas, and has graduated more than 35 Ph.D. students.

Dr. Cutkosky is a former Fulbright Chair, Anderson Faculty Scholar, and NSF Presidential Young Investigator. He is a member of American Society of Mechanical Engineers.